Energy Extraction from a Pitching-Plunging Airfoil

Manuel García Lucas
ISAE-SUPAERO, Université de Toulouse, 31055 Toulouse, FRANCE

The energy extraction capabilities of an airfoil performing oscillatory pitching and plunging motions in turbulent conditions are studied by means of two-dimensional, unsteady CFD simulations. A parametric study in the non-dimensional frequency – pitch amplitude space has been conducted in order to find the conditions that yield the highest power coefficient and efficiency. A maximum mean power coefficient of 1.045 has been obtained for a non-dimensional frequency of 0.15 and a pitch amplitude of 75 deg. This corresponds to a mean power of 1.24 kW extracted in one cycle and an efficiency of 39.24%.

Nomenclature

c	=	chord length, m
d	=	vertical distance swept by the airfoil, m
f	=	frequency of oscillation, Hz
f^*	=	non-dimensional frequency
h	=	vertical displacement of the pitch axis, m
H_0	=	plunge amplitude, m
M	=	moment about the pitch axis, N m
P	=	total power extracted, kW
P_a	=	total power available, kW
P_y	=	plunging contribution to P, kW
P_θ	=	pitching contribution to P, kW
Re	=	Reynolds number
t	=	time, s
T	=	period of oscillation of frequency f, s
U_∞	=	free stream velocity, m/s
V_{eff}	=	effective upstream velocity, m/s
V_y	=	plunge or vertical velocity, m/s
x_p	=	chordwise position of the pitch axis, m
y_{TE}	=	vertical position of the trailing edge, m
Y	=	force in the vertical direction, N
α	=	effective angle of attack, deg
$\alpha_{T/4}$	=	quarter-period effective angle of attack, deg
η	=	efficiency
ϕ	=	phase shift between pitch and plunge, deg
θ	=	angular position of the chord axis, deg
θ_0	=	pitch amplitude, deg
χ	=	feathering parameter
Ω	=	pitch or rotation velocity, rad/s
C	=	non-dimensional coefficient
$\bar{}$	=	mean value over one or more periods
$\widehat{}$	=	peak value over one or more periods

I. Introduction

Over the last decades, scientists have been searching for new ways of producing clean, renewable energy. This need for a sustainable energy supply is further heightened by the recent rise in fossil fuel prices [1]. Furthermore, both wind and hydraulic energy have been proven to be ecological, yet efficient sources of energy [2, 3].

It is known that an airfoil performing oscillatory pitching and plunging motions can either produce thrust or extract energy [4, 5]. Given the aforementioned context, this work investigates the energy extraction capabilities of such a device in turbulent conditions.

Since using an oscillating airfoil to extract energy is a relatively recent proposal, brought by the pioneering study of McKinney and DeLaurier in 1981 [5], there is no extensive literature on the subject. For this reason, the previous research has some limitations: either laminar flow was considered, like Kinsey and Dumas did [4]; or low amplitudes and frequencies of oscillation were used, as Akhlaghi et al. did [6]; or energy extraction regimes were not explored and the authors only focused on thrust generation.

In this work, a parametric study in the frequency – pitch amplitude space has been conducted by means of two-dimensional, unsteady CFD simulations, with a focus on energy extraction. Turbulent conditions have been considered thanks to a Reynolds number of 5×10^5. Furthermore, high pitch amplitudes (from 15 to 90 deg) and frequencies of oscillation (non-dimensional frequencies from 0.05 to 0.25) have been reached. This allows for unsteady stall to occur, which amplifies the value of the force coefficients.

Some of the possible applications of this investigation are wind energy extraction, e.g. a fluttering wing with pitch control, and hydraulic energy extraction. For the latter, the presented contraption offers several benefits according to Jones et al. [7]. First of all, a dam is not required; therefore, costs and environmental impact are reduced. Second, it can function in relatively shallow waters and it can be fitted between the pilings of existing bridges. Finally, the flow

of water in a river is more consistent and reliable than the wind. Although the simulated fluid in this study is air, the analyzed configuration would be equivalent in terms of Reynolds number to a square channel of side 20 cm with water flowing at 1 m/s.

II. Theoretical background

A. Motion description

The position of the airfoil can be expressed through the angular position of its chord axis (θ) and the vertical displacement of its pitch axis (h), which are defined periodically over time with a phase difference ϕ:

$$\theta(t) = \theta_0 \sin(2\pi f t)$$
$$h(t) = H_0 \sin(2\pi f t + \phi)$$

These parameters can be seen in Fig. 1.

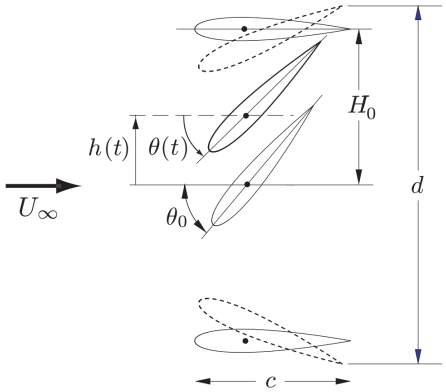

Figure 1 Imposed pitching and plunging motions [4]

Deriving, the pitch (or rotation) and the plunge (or vertical) velocities are obtained:

$$\Omega(t) = 2\pi f \theta_0 \cos(2\pi f t)$$
$$V_y(t) = 2\pi f H_0 \cos(2\pi f t + \phi)$$

B. Operating regimes

This oscillating airfoil can operate in two different regimes, either power extraction or propulsion. This mainly depends on the direction of the forces generated by the flow on the airfoil.

In the power extraction regime, the vertical force is in the same direction as the vertical displacement, i.e. the vertical force and the plunge velocity have the same sign. The work produced by the flow on the airfoil is positive; thus, power can be extracted.

In the propulsion regime, the horizontal force is in the same direction as the airfoil's apparent horizontal movement, this is, in the opposite direction to U_∞. Therefore, there is a net propulsion at the expense of doing some work on the fluid, since Y is opposed to the vertical displacement.

The imposed motion induces an effective velocity (V_{eff}) and an effective angle of attack (α), which are defined as follows:

$$V_{\text{eff}}(t) = \sqrt{U_\infty^2 + V_y(t)^2}$$
$$\alpha(t) = \arctan\left(-\frac{V_y(t)}{U_\infty}\right) - \theta(t)$$

The maximum effective velocity is obtained at the quarter period, and the maximum effective angle of attack is approximated by the absolute value of its quarter-period value:

$$\widehat{V}_{\text{eff}} = V_{\text{eff}}(T/4) = \sqrt{U_\infty^2 + (2\pi f H_0)^2}$$
$$\widehat{\alpha} \approx |\alpha_{T/4}| = |\alpha(T/4)| = \left|\arctan\left(\frac{2\pi f H_0}{U_\infty}\right) - \theta_0\right|$$

One defines the feathering parameter as:

$$\chi = \frac{\theta_0}{\arctan\left(\dfrac{2\pi f H_0}{U_\infty}\right)}$$

According to Kinsey and Dumas [4]:

> Based on a simple quasi-steady argument, which leads to necessary but not precisely sufficient conditions [...] $\chi < 1$ is associated to propulsion ($\alpha_{T/4} > 0$), while $\chi > 1$ corresponds to power extraction ($\alpha_{T/4} < 0$).

Figure 2 shows the motion of the airfoil in both operating regimes.

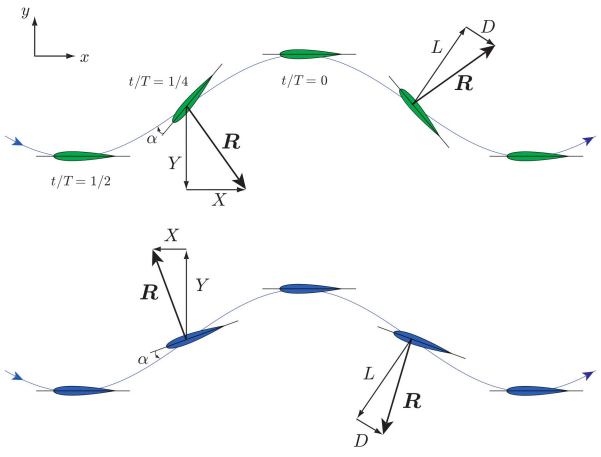

Figure 2 Oscillating airfoil regimes: power extraction (above, $\alpha_{T/4} < 0, \chi > 1$) and propulsion (below, $\alpha_{T/4} > 0, \chi < 1$) [4]

C. Extracted power and efficiency

Remark. The definitions for the power coefficient and the efficiency used by Kinsey and Dumas [4] and Young et al. [8, 9] are employed in this paper.

The power extracted from the flow is calculated as the sum of the contribution from the pitching motion (P_θ) and that from the plunging motion (P_y):

$$\begin{cases} P_\theta(t) = M(t)\Omega(t) \\ P_y(t) = Y(t)V_y(t) \end{cases} \Rightarrow P(t) = P_\theta(t) + P_y(t)$$

These contributions can be written as a function of dimensionless power coefficients:

$$C_{P_\theta}(t) = \frac{P_\theta(t)}{\frac{1}{2}\rho U_\infty^3 c} = \frac{M(t)}{\frac{1}{2}\rho U_\infty^2 c^2}\frac{\Omega(t)c}{U_\infty} = C_M(t)\frac{\Omega(t)c}{U_\infty}$$

$$C_{P_y}(t) = \frac{P_y(t)}{\frac{1}{2}\rho U_\infty^3 c} = \frac{Y(t)}{\frac{1}{2}\rho U_\infty^2 c}\frac{V_y(t)}{U_\infty} = C_Y(t)\frac{V_y(t)}{U_\infty}$$

The total power coefficient is $C_P(t) = C_{P_\theta}(t) + C_{P_y}(t)$.

Finally, the total power available in the flow is expressed as:

$$P_a = \frac{1}{2}\rho U_\infty^3 d \Rightarrow C_{P_a} = \frac{P_a}{\frac{1}{2}\rho U_\infty^3 c} = \frac{d}{c}^*$$

The efficiency is then calculated as the ratio of the mean power extracted during a period to the total power available:

$$\eta = \frac{\overline{P}}{P_a} = \frac{\overline{C}_P}{C_{P_a}} = \frac{\overline{C_{P_\theta} + C_{P_y}}}{C_{P_a}}$$

According to the study performed by Betz [10], the maximum power that can be extracted from the wind is theoretically limited to an efficiency of $16/27 \approx 59.3\%$, regardless of the type of turbine used. However, actual wind turbines can reach an efficiency up to 47% [11], which is approximately 80% of the Betz limit.

D. Literature review

Young et al. [8, 9] carried out a more complete theoretical analysis in which they accounted for effects such as unsteadiness, work by viscous forces, viscous dissipation and fluctuating forces on the turbine plane that were not considered in the original Betz's analysis. In this way, it was shown that there exist numerical combinations that would yield an efficiency that exceeds the Betz limit. However, it was not trivial to find a physically plausible combination. In fact, the authors found that in practice the Betz limit cannot be violated: although the extra energy required can be generated by the unsteady behavior of the vortices, it is not used and escapes downstream. In their numerical simulations, a maximum efficiency of 34.1% was obtained through direct measurements and 33.8% using a control volume approach.

In their pioneering work, McKinney and DeLaurier [5] conducted an analytical and experimental investigation of a windmill that utilized an oscillating wing to extract energy: the "wingmill". Efficiencies comparable to those of rotatory designs were achieved, as high as 16.8% for $\theta_0 = 30\,\text{deg}$ and $U_\infty = 8.0\,\text{m/s}^\dagger$. It was observed that the extracted power peaks at a phase of 110 deg and the efficiency at 90 deg. For this reason, a phase of 90 deg has been used in most of the subsequent studies, as well as in the present one.

Finally, Kinsey and Dumas [4] performed a parametric study in the frequency – pitch amplitude space ($f^* = 0$–0.25, $\theta_0 = 0$–$90\,\text{deg}$), considering laminar conditions (Re = 1100) and maintaining a constant plunge amplitude of one chord and a phase of 90 deg. Efficiencies up to 33.7% were obtained for high pitch amplitudes within 70–80 deg and non-dimensional frequencies in the range of 0.12–0.18. Moreover, it was observed that motion-related parameters (f^* and θ_0) have the strongest effects on performances, whereas geometric and viscous parameters play a secondary role. Furthermore, it was stated that leading edge vortex shedding (LEVS) is necessary to achieve a good synchronization between the vertical force and the plunge velocity. This investigation is the inspiration for this work.

III. Numerical setup

A. Geometry and computational domain

In this study, the airfoil analyzed by Akhlaghi et al. [6] has been employed (Fig. 3), with a chord of 0.25 m and its pitch axis located at one quarter of the chord.

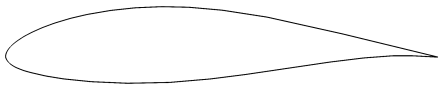

Figure 3 Airfoil geometry (coordinates available in the article written by Akhlaghi et al. [6])

As for the computational domain, its shape and measurements have been taken from the work of Kesarwani et al. and it can be seen in Fig. 4.

*The calculation of d is detailed in the Appendix.

†The efficiencies from the original document were multiplied by $16/27$ in order to "translate" them to the current definition.

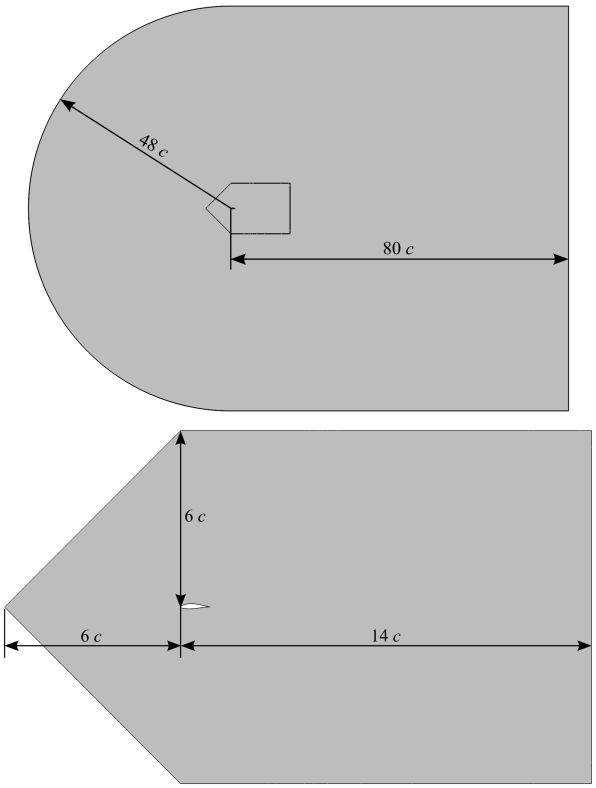

Figure 4 Computational domain with measurements of the base domain (top) and overset domain with its measurements (bottom). Measurements are taken from the leading edge

B. Models and fluid properties

A two-dimensional flow model has been imposed to carry out the two-dimensional simulations.

Regarding the simulated fluid, air with constant density (1.8515 $\mathrm{kg/m^3}$) and dynamic viscosity (1.85508×10^{-5} Pa s) has been used. These are the default values from STAR CCM+, which is the software employed to perform the simulations.

Turbulence has been modeled through the Reynolds-Averaged Navier-Stokes equations, making use of the SST k-Omega turbulence model and the Gamma transition model.

C. Solver

A segregated-flow, implicit, unsteady solver with 2nd-order temporal discretization has been employed, with a time discretization of 2,000 time steps per period and 25 inner iterations per step.

As for the under-relaxation factors, they have been left to their default values since convergence was not a problem once the correct mesh and time discretization had been chosen.

D. Boundary and initial conditions

Two regions have been defined: a base region, with a velocity inlet of 20 m/s and a pressure outlet of 0 Pa; and a moving overset region with its corresponding overset interface, as well as two no-slip wall boundaries to define the airfoil's pressure and suction sides. These boundaries are shown in Fig. 5.

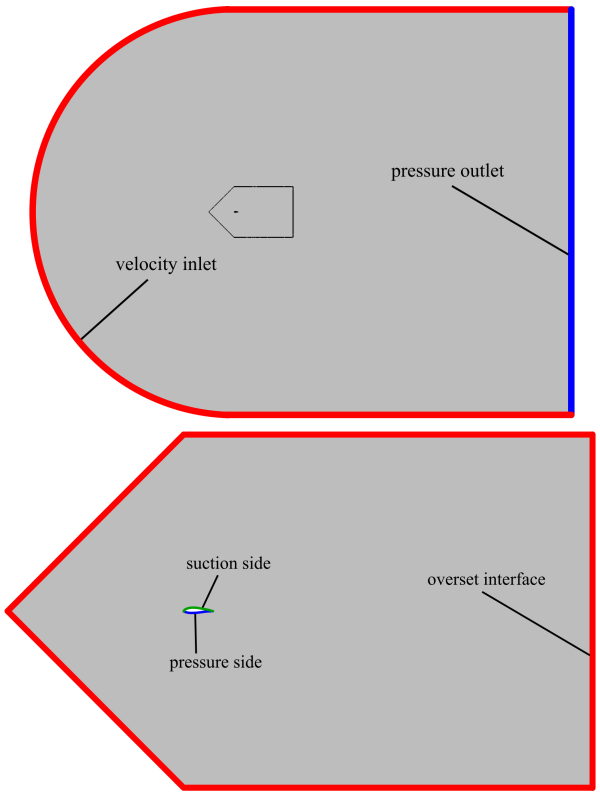

Figure 5 Boundaries of the base region (top) and of the overset region (bottom)

Regarding the initial conditions, the same values as for the boundary conditions have been used.

E. Meshing strategy

There are two regions; therefore, two different meshes have been employed. The structured mesh *fine22* from Kesarwani et al. [12] has been used as the base or background mesh. Regarding the overset mesh, a two-dimensional, unstructured, polyhedral mesh has been created.

The motion of the airfoil has been imposed on this overset region. In this way, the information from the donor cells of the overset mesh (those in the overset interface) is communicated to the receptor cells of the background mesh, while the background cells covered by the overset region stay inactive.

The said mesh has been refined in areas such as the airfoil surface, the trailing edge and the wake. A prism layer has been implemented as well. The resulting overset mesh

of 48,838 cells is shown in Fig. 6 and its characteristics are detailed in Table 1.

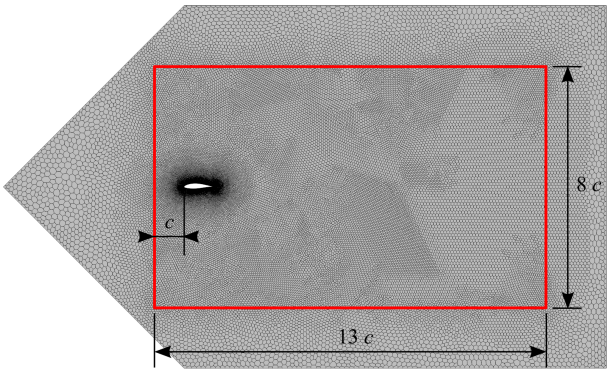

Figure 6 Mesh in the overset region. Wake refinement region in red with its measurements

Table 1 Overset mesh characteristics

Mesh part or refinement	Target size, mm	Minimum size, mm	Growth rate
Default	19.39	4.847	1.05
Airfoil	1.212	0.6059	1.05
Trailing edge	1.212	–	–
Interface	40.00	9.694	1.10
Wake	19.39	–	–

IV. Independence analyses

The mean horizontal force coefficient $\overline{C}_X$, the maximum vertical force coefficient $\widehat{C}_Y$, the maximum moment coefficient $\widehat{C}_M$, and the mean power coefficient $\overline{C}_P$ over the last two simulated periods have been used to conduct the independence studies.

Convergence has been considered once the variation of all these parameters in absolute value was below 5%.

A. Mesh independence

For the mesh independence study three overset meshes were created, with 21,656, 48,838, and 110,323 cells in the overset region (named *mesh022k*, *mesh049k* and *mesh110k*, respectively).

The results of the mesh independence study are shown in Table 2.

Table 2 Results of the mesh independence study. The variation with respect to the previous mesh is in parentheses

Overset mesh	$\overline{C}_X$	$\widehat{C}_Y$
mesh022k	2.178	3.204
mesh049k	2.225 (+2.16%)	3.630 (+13.3%)
mesh110k	2.229 (+0.192%)	3.784 (+4.25%)
Overset mesh	$\widehat{C}_M$	$\overline{C}_P$
mesh022k	0.7562	0.9281
mesh049k	0.9909 (+31.0%)	1.045 (+12.6%)
mesh110k	1.038 (+4.74%)	1.016 (−2.76%)

According to the convergence criterion, the mesh *mesh049k* has been employed for the time step independence analysis and for the parametric study.

Furthermore, the pressure coefficient distribution on the airfoil surface has been represented for the different overset meshes in Fig. 7. We observe that the result converges with an increasing number of cells and that the chosen mesh *mesh049k* provides a very similar pressure coefficient distribution to that of the finest mesh.

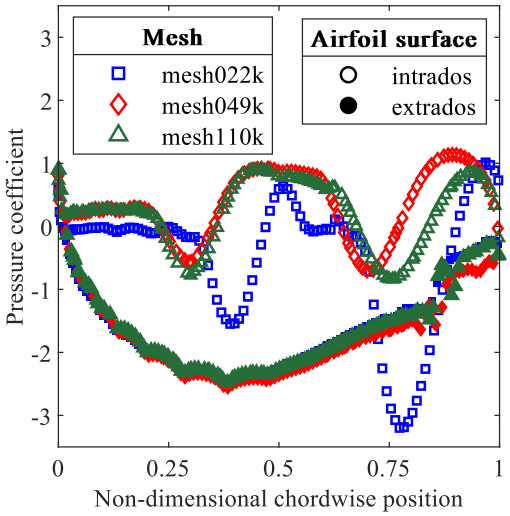

Figure 7 Pressure coefficient distribution on the airfoil surface at the end of a cycle ($t = T$) for the different overset meshes

B. Time step independence

Regarding the time step independence study, simulations with 125, 250, 500, 1,000, 2,000 and 4,000 time steps per period have been carried out. The results are presented in Table 3.

Table 3 Results of the time step independence study. The variation with respect to the previous time discretization is in parentheses. TSPP stands for "time steps per period"

TSPP	$\overline{C}_X$	$\widehat{C}_Y$
125	2.198	3.489
250	2.215 (+0.766%)	3.346 (−4.11%)
500	2.214 (−0.0614%)	3.984 (+19.1%)
1,000	2.226 (+0.573%)	3.665 (−8.00%)
2,000	2.225 (−0.0729%)	3.630 (−0.960%)
4,000	2.222 (−0.129%)	3.478 (−4.19%)

TSPP	$\widehat{C}_M$	$\overline{C}_P$
125	1.102	0.9605
250	0.9550 (−13.4%)	1.034 (+7.63%)
500	1.027 (+7.58%)	0.9754 (−5.65%)
1,000	1.148 (+11.8%)	1.015 (+4.10%)
2,000	0.9925 (−13.6%)	1.045 (+2.87%)
4,000	1.043 (+5.07%)	1.063 (+1.74%)

A time discretization of 2,000 time steps per period has been chosen for the parametric study, although the convergence criterion is slightly exceeded for the maximum moment coefficient.

To complete the time step independence study, the power spectral difference (PSD) of the pressure at a given point of the wake has been represented in Fig. 8. It is observed that, especially for lower frequencies (below 100 Hz), the PSD for 2,000 TSPP offers a good resemblance to that for 4000 TSPP.

V. Validation

As a result of the scarcity of experimental data to compare with, the validation has been performed using the experimental results of Akhlaghi et al. [6] for a pitch amplitude of 5 deg and a non-dimensional frequency of 0.0127, even if these conditions are far from those simulated in the parametric study.

Simulations with different mean effective angles of attack have been conducted for both constructive ($\phi = -\pi/6$) and destructive ($\phi = 5/6$) motions in order to compare the hysteresis loops of both works. This comparison is shown in Fig. 9.

The current results closely follow the experimental ones for the constructive case, whereas they deviate slightly for the destructive motion. Note that the present results are closer to the static lift coefficient – effective angle of attack curve than the experimental ones.

For high angles of attack, there are more significant differences in both constructive and destructive motions, maybe due to numerical errors and instabilities caused by stall. It can be seen that the hysteresis loop for $\overline{\alpha} = 15$ deg diverges, which is reasonable due to stall.

This procedure is expected to validate the present mesh, time step size and overall strategy. However, to be sure that the results are reliable when simulating the conditions of the parametric study, validation with experimental data in more similar conditions would be necessary, but unfortunately this is something we do not dispose of at the moment.

VI. Parametric study

A. Definition of the parametric study

According to Kinsey and Dumas [4]:

> Increasing [...] the heaving amplitude H_0 (everything else being the same), inevitably moves us toward the feathering limit[‡] [...]. This ultimately has a detrimental effect past a certain level.

For this reason and due to time constraints, it has been decided to conduct the study in the f^*–θ_0 parametric space, leaving a constant plunge amplitude of one chord. The ranges of non-dimensional frequencies and pitch amplitudes studied are $f^* = 0.05$–0.25 (in steps of 0.05), $\theta_0 = 15$–90 deg (in steps of 15 deg).

B. Results: power coefficient and efficiency

The results of the parametric study in terms of power coefficient and efficiency are presented in Fig. 10. Simulations have been performed for each (f^*, θ_0) pair represented by a dot, then the results have been interpolated to create the contours using splines, by means of the `interpolate` function from MATLAB.

Taking into consideration these simulations, the optimal configuration is a non-dimensional frequency of 0.15 (which translates to a frequency of oscillation of 12 Hz in the simulated case) and a pitch amplitude of 75 deg. This is in accordance to what Kinsey and Dumas obtained. These conditions yield a mean power coefficient of 1.045, which corresponds to a mean power of 1.24 kW extracted during the cycle and an efficiency of 39.24%.

Nevertheless, according to the interpolation, the power coefficient could potentially reach a value of 1.1 and the efficiency would then be 40.65%.

[‡]The feathering limit is the point at which $\chi = 1$; therefore, neither power is extracted nor thrust is generated.

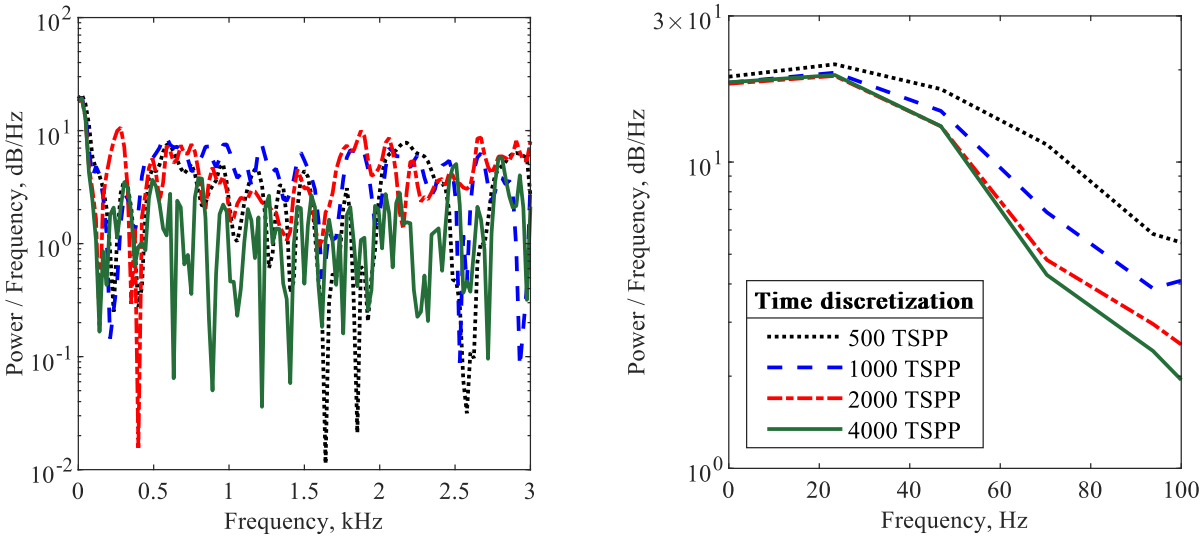

Figure 8 Power spectral density of the pressure at a point in the wake one chord downstream of the trailing edge for different time discretizations (125 and 250 TSPP have been omitted for the sake of clarity). Full range of frequencies (left) and detail up to a frequency of 100 Hz (right)

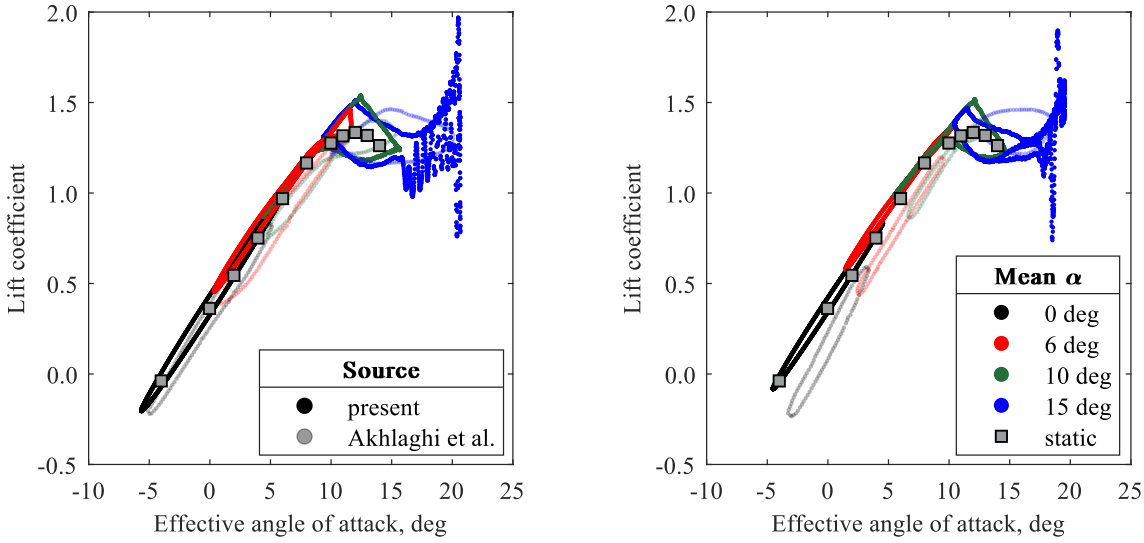

Figure 9 Comparison of the hysteresis loops of the present study with the experimental results of Akhlaghi et al. [6] for a pitch amplitude of 5 deg and different mean effective angles of attack, for both constructive (left) and destructive (right) motions

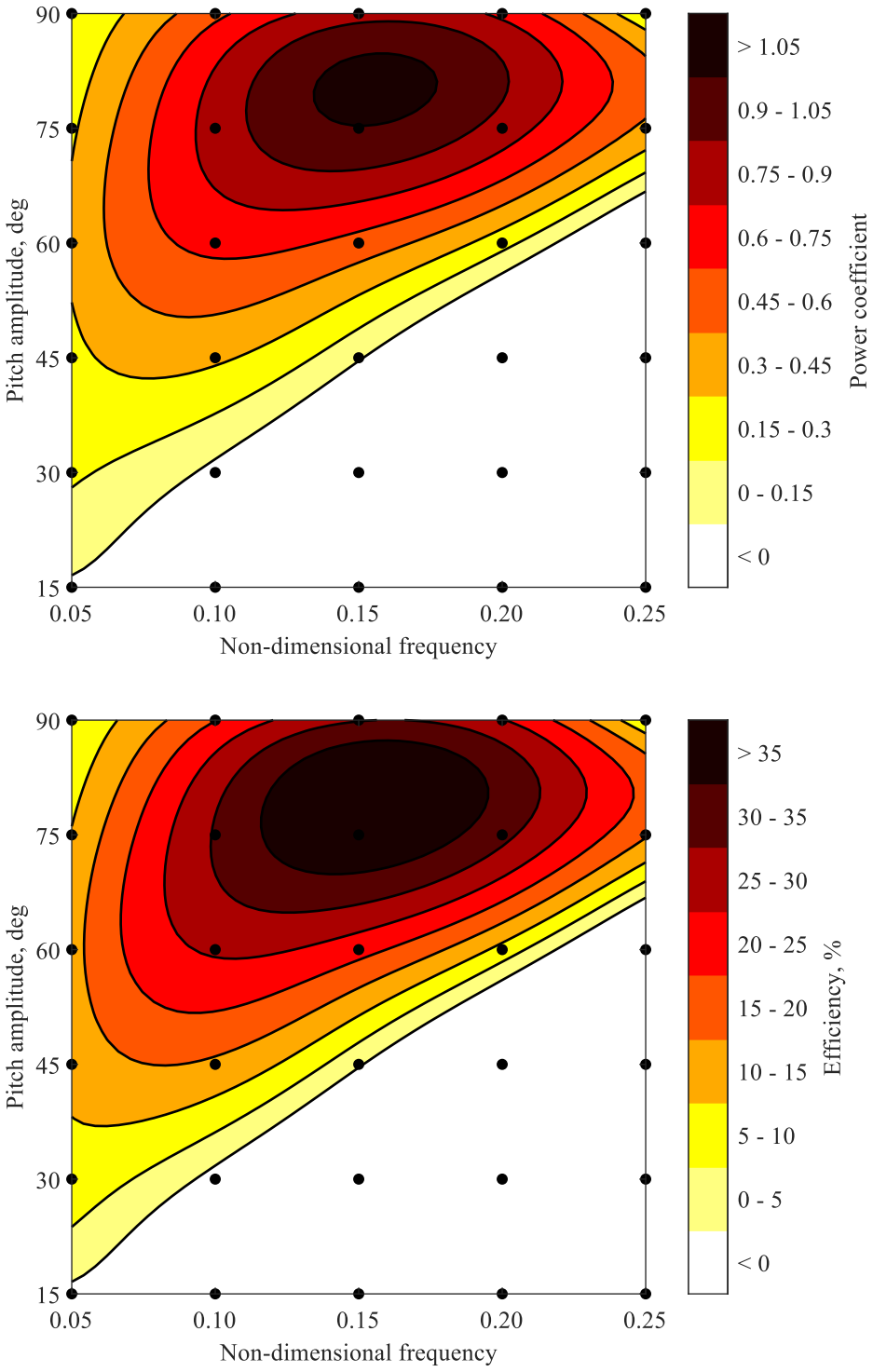

Figure 10 Power coefficient (top) and efficiency (bottom) contours for different pitch amplitudes and non-dimensional frequencies. Note that the maximum efficiency is bounded by the Betz limit at 59.3%

C. Comparison between cases

Three cases with the same non-dimensional frequency of 0.15 and different pitch amplitudes have been compared: $\theta_0 = 30$ deg (negative mean power), $\theta_0 = 45$ deg (mean power close to zero), and $\theta_0 = 75$ deg (maximum mean power). The power coefficient profiles for these three cases are shown in Fig. 11.

Here follows a description of the flow characteristics (velocity and vorticity) of these three cases in order to understand these large differences in performance.

1. Velocity field (Fig. 12)

For a pitch amplitude of 30 deg, the movement is clearly dominated by the plunging motion. When going down, the airfoil has a positive effective angle of attack (positive lift), and the contrary occurs when going up. In this manner, the vertical force is always opposite to the plunge velocity, so the power coefficient is always negative.

When the pitch amplitude is 45 deg, pitching and plunging motions balance each other. Both in the climbing and descending motion, a negative lift is produced in the upper part of the movement whereas a positive lift is generated in the lower part (C_Y and V_y have the same sign for $t/T = 0$–0.25 and $t/T = 0.5$–0.75 and opposite sign otherwise). Therefore, positive and negative contributions are compensated, and the mean power coefficient is close to zero.

In the most efficient case (pitch amplitude of 75 deg), the movement is dominated by the pitching motion. The pitch rate counters the effect of the plunge velocity in the leading edge of the airfoil, which increases the velocity difference between the leading and the trailing edge. This in turn increases the vertical force (in absolute value) thanks to the large pitch amplitude. As a consequence, $C_Y > 0$ when going up and $C_Y < 0$ when going down. This yields a positive power coefficient throughout the whole cycle.

2. Vorticity field (Fig. 13)

For pitch amplitudes of 30 and 45 deg, no remarkable effects are observed. Almost all of the wake is contained inside the distance swept by airfoil (d), i.e. little to no flow is dragged from the exterior of the wake.

However, when the pitch amplitude is 75 deg, there is a great contribution to vorticity due to LEVS, which is the cause of the synchronization between Y and V_y according to Kinsey and Dumas [4]. This vortex is reattached due to the motion of the airfoil. For this reason, dynamic stall is delayed according to Khalid et al. [13]. Vortexes are pushed well outside d; as a result, a lot of fluid is dragged from the exterior inside the wake. It can be observed that the downwash flow is slowed down due to the counter rotating vortices. This reduction in velocity can also be seen on the velocity field. This loss of kinetic energy is typical in power extraction mechanisms due to the conservation of momentum.

VII. Conclusion

It can be concluded that turbulent conditions provide, with respect to laminar ones, a much higher power coefficient (21.5% higher according to the simulations, 28% according to the interpolation) and a higher efficiency (16.4% higher according to the simulations, 20.6% according to the interpolation).

A non-dimensional frequency of 0.15 and a pitch amplitude of 75 deg are found to be the optimal conditions for energy extraction (0.156 and 79.8 deg according to the interpolation).

However, there are some limitations to be mentioned. On the one hand, time constraints and computational cost have been limiting factors: a more in-depth analysis could have been carried out in order to consider three-dimensional effects, to evaluate the influence of the plunge amplitude and the phase, and to perform more simulations in the high-performance region. On the other hand, it would be interesting to assess the feasibility of such high frequencies and amplitudes in terms of structural stress and stability.

Regarding future work, it could be oriented to conducting a similar study using two airfoils in tandem configuration, since Young et al. showed a 90% increase in efficiency in laminar conditions [9]. A similar improvement is expected to take place in a turbulent case.

Appendix: Calculation of d

To find the total distance swept by the airfoil, first one maximizes the vertical position of the trailing edge:

$$y_{TE}(t) = h(t) + \left(1 - \frac{x_p}{c}\right) c \sin(\theta(t))$$

Once this distance is found, it is doubled to find d. The values of d for the studied pitch amplitudes are shown in Table 4.

Table 4 Values of the total distance swept by the trailing edge for different pitch amplitudes

Pitch amplitude, deg	Distance swept, m
15	0.5095
30	0.5367
45	0.5767
60	0.6218
75	0.6654
90	0.7036

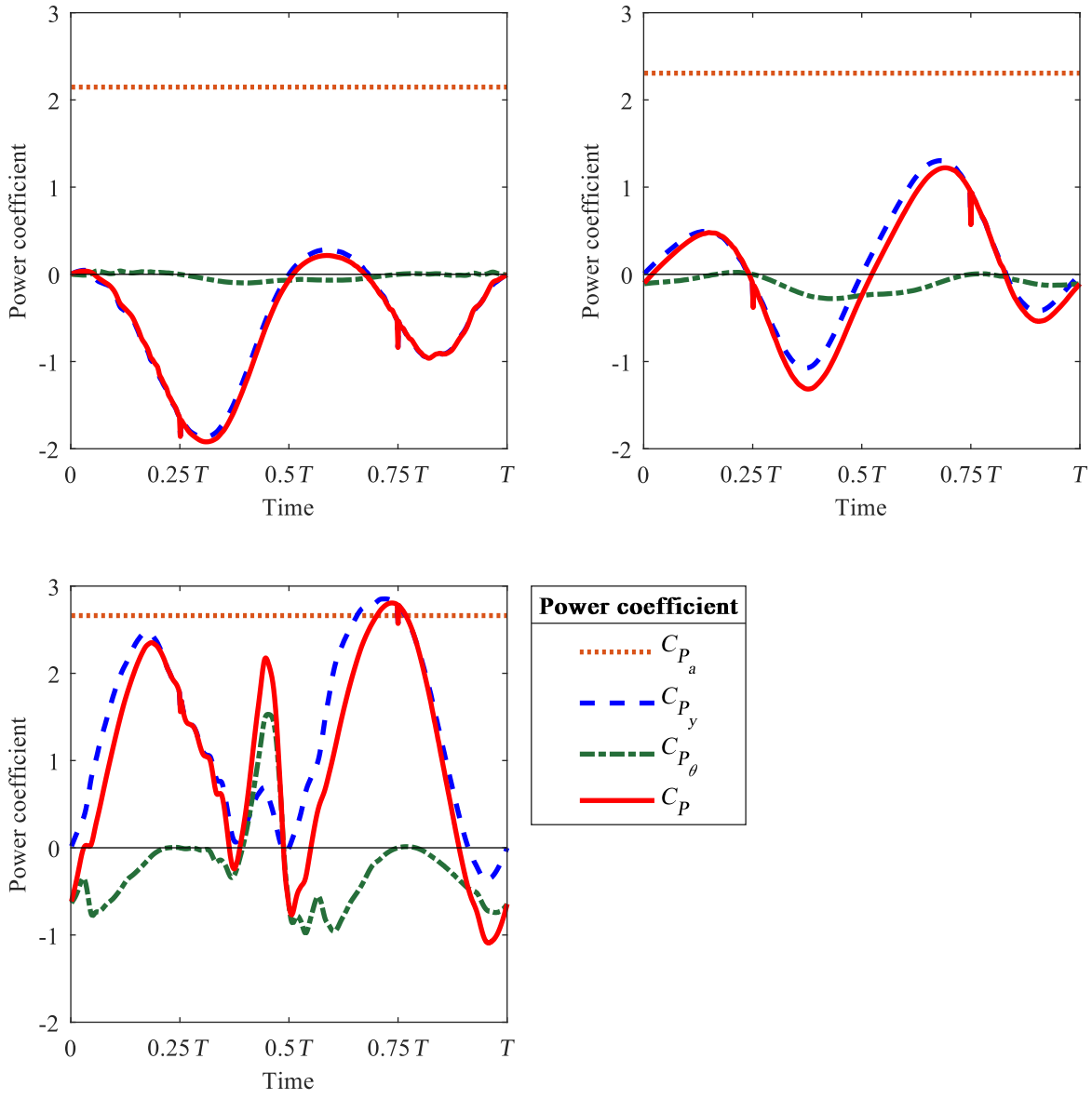

Figure 11 Power coefficients for a non-dimensional frequency of 0.15 and different pitch amplitudes: 30 deg (negative power, top left), 45 deg (null power, top right) and 75 deg (maximum power, bottom)

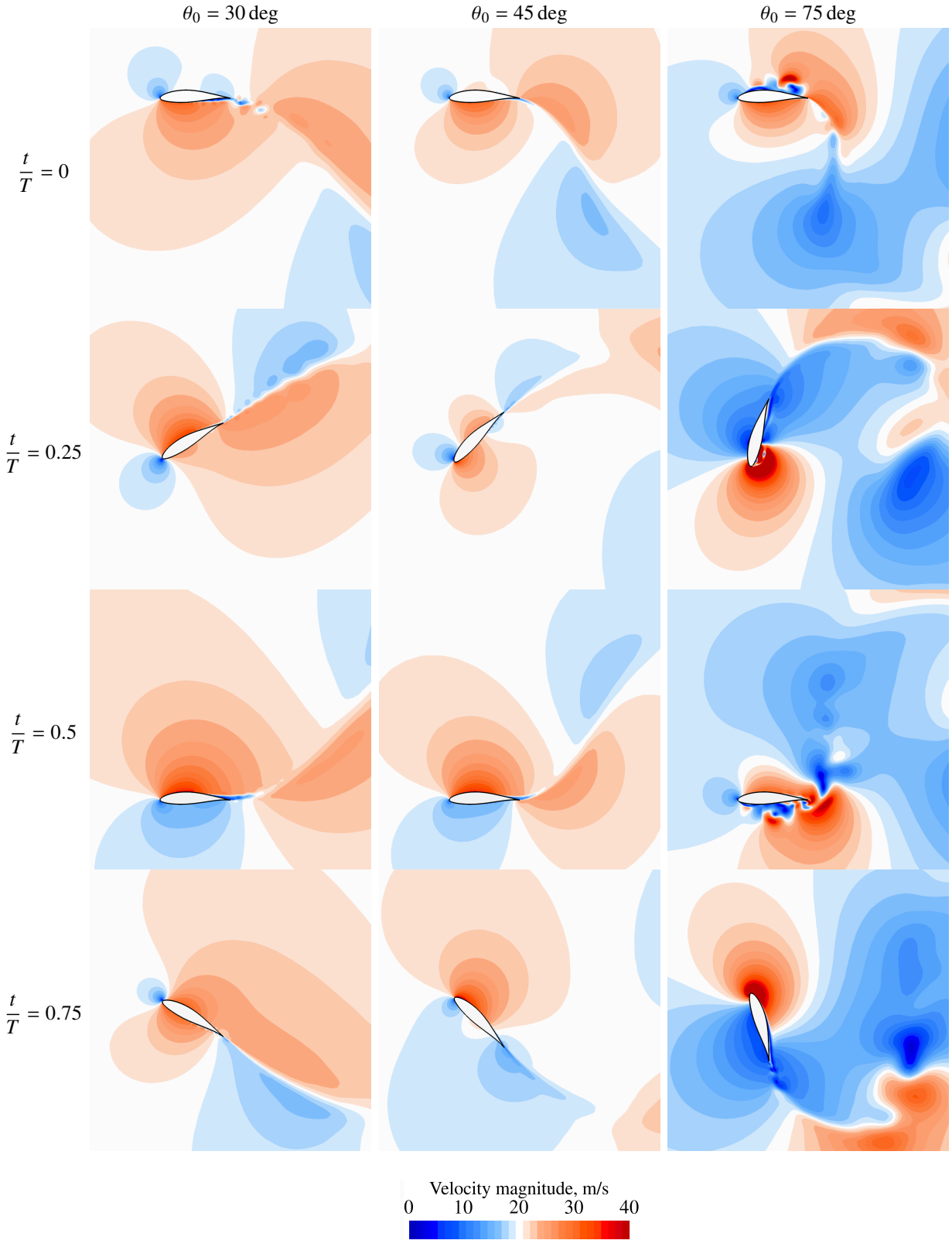

Figure 12 Velocity magnitude contours for a non-dimensional frequency of 0.15 and different pitch amplitudes (30 deg, 45 deg and 75 deg) in different instants of the cycle

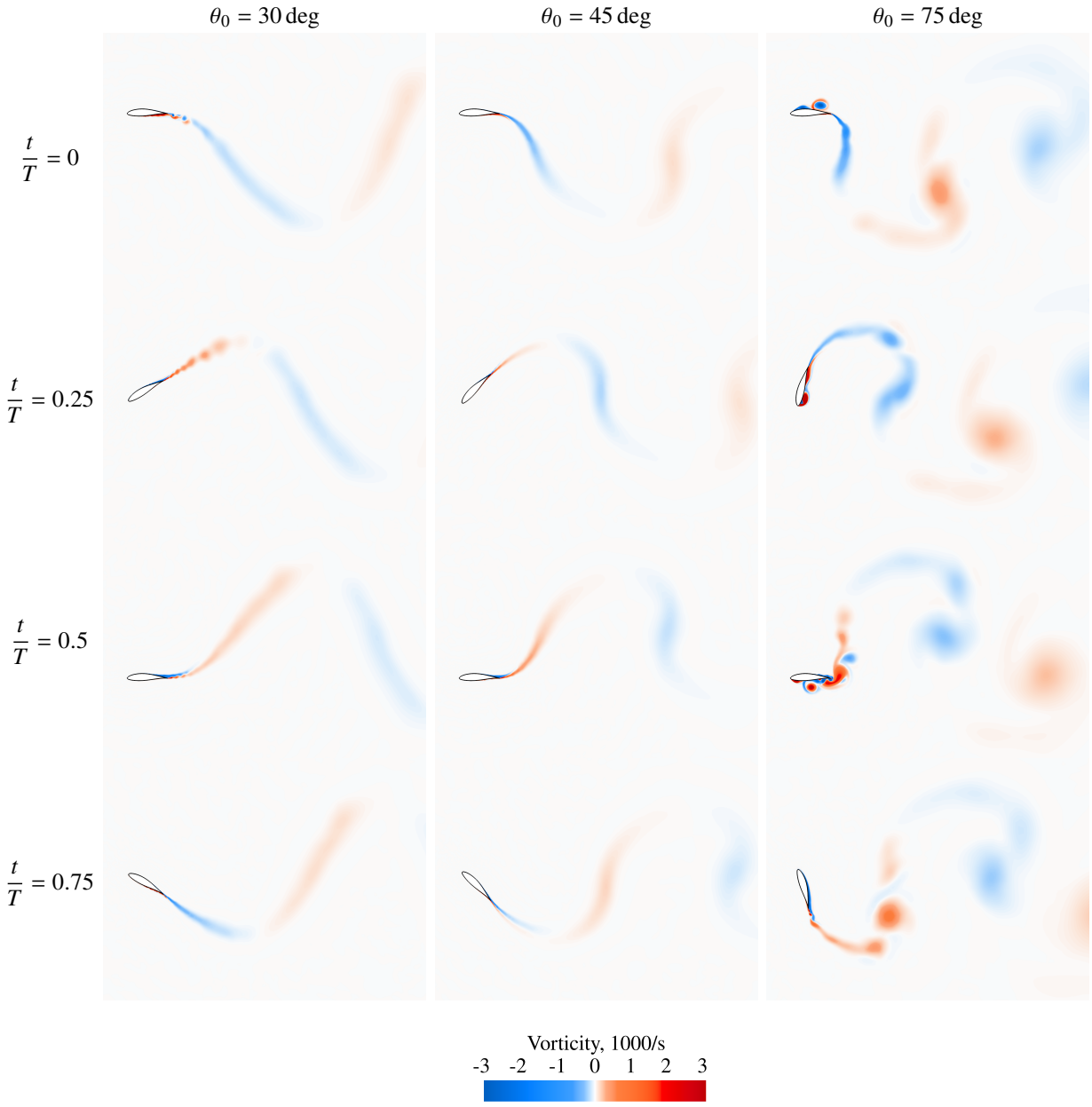

Figure 13 Vorticity contours for a non-dimensional frequency of 0.15 and different pitch amplitudes (30 deg, 45 deg and 75 deg) in different instants of the cycle. Red for positive vorticity (counter-clockwise direction), blue for negative vorticity (clockwise direction)

References

[1] United Nations Environment Programme, "As oil prices spike, new investments in fossil fuels could be disastrous – UNEP expert," https://www.unep.org/news-and-stories/story/oil-prices-spike-new-investments-fossil-fuels-could-be-disastrous-unep, 2022. Accessed: 2022-07-29.

[2] Office of Energy Efficiency & Renewable Energy, "Advantages and Challenges of Wind Energy," https://www.energy.gov/eere/wind/advantages-and-challenges-wind-energy, circa 2014. Accessed: 2022-07-29.

[3] United Nations Environment Programme, "Benefits of Hydropower," https://www.energy.gov/eere/water/benefits-hydropower, circa 2014. Accessed: 2022-07-29.

[4] Kinsey, T., and Dumas, G., "Parametric Study of an Oscillating Airfoil in Power Extraction Regime," *Aiaa Journal - AIAA J*, Vol. 46, 2008, pp. 1318–1330. https://doi.org/10.2514/1.26253.

[5] McKinney, W., and DeLaurier, J., "Wingmill: An Oscillating-Wing Windmill," *Journal of Energy*, Vol. 5, No. 2, 1981, pp. 109–115. https://doi.org/10.2514/3.62510.

[6] Akhlaghi, H., Soltani, M.-R., and Maghrebi, M.-J., "Transitional boundary layer study over an airfoil in combined pitch-plunge motions," *Aerospace Science and Technology*, Vol. 98, 2020, p. 105694. https://doi.org/https://doi.org/10.1016/j.ast.2020.105694.

[7] Jones, K. D., Davids, S., and Platzer, M. F., "Oscillating-Wing Power Generator," *ASME/JSME Joint Fluids Engineering Conference*, San Francisco, California, 1999.

[8] Young, J., Tian, F.-B., and Lai, J. C. S., "Betz analysis of a single flapping foil power generator," *First International Symposium on Flutter and its Application*, 2016, pp. 485–494.

[9] Young, J., Tian, F.-B., Liu, Z., Lai, J. C. S., Nadim, N., and Lucey, A. D., "Analysis of unsteady flow effects on the Betz limit for flapping foil power generation," *Journal of Fluid Mechanics*, Vol. 902, 2020, p. A30. https://doi.org/10.1017/jfm.2020.612.

[10] Betz, A., "Schraubenpropeller mit geringstem Energieverlust. Mit einem Zusatz von l. Prandtl," *Nachrichten von der Gesellschaft der Wissenschaften zu Göttingen, Mathematisch-Physikalische Klasse*, Vol. 1919, 1919, pp. 193–217. URL http://eudml.org/doc/59049.

[11] Burton, T., Sharpe, D., Jenkins, N., and Bossanyi, E., *The Wind Energy Handbook*, 2001, Vol. 1, Chap. 4, pp. 173–174. https://doi.org/10.1002/0470846062.

[12] Kesarwani, A., Sundararaman, A., Jain, R., and Galal, M., "Transitional Boundary layer on a Pitching-plunging airfoil," , February 2021. Numerical Fluid Mechanics (ISAE-SUPAERO), unpublished.

[13] Khalid, M., Imran, A., and Durrani, N., "Analysis of Strouhal Number Based Equivalence of Pitching and Plunging Airfoils and Wake Deflection," *Proceedings of the Institution of Mechanical Engineers, Part G: Journal of Aerospace Engineering*, Vol. 229, 2014. https://doi.org/10.1177/0954410014551847.